Algorithms for American XVA and free boundary calculations with stochastic counterparty default intensity

Yuwei Chen and Christina C. Christara
Department of Computer Science
University of Toronto
Toronto, Ontario M5S 2E4, Canada
{ywchen,ccc}@cs.toronto.edu

Abstract

Credit and total valuation adjustments (CVA and XVA) are significant in equity markets, as parts of the risk management under Basel III framework. In addition, path-dependent derivatives, such as American-type ones, are heavily traded in markets. Therefore, it is important to accurately and efficiently compute valuation adjustments for American-type derivatives. In this paper, we derive a two-dimensional (2D) in space partial differential equation (PDE) for pricing American-type derivatives including the XVA, assuming the counterparty default risk follows a mean-reversion stochastic process, while the self-party has constant default risk. We reformulate the time-dependent, 2D nonlinear PDE into penalty form, which includes two nonlinear source terms. We employ the double-penalty iteration for the 2D PDE to resolve the two nonlinear terms, while we use a finite difference scheme for the spatial discretization, and Crank-Nicolson-Rannacher timestepping. We introduce algorithms for the accurate calculation of the free boundary. We also formulate an asymptotic approximation technique, similar to the one developed for the European case problem, but adjusted for the American put option problem. A key step is to derive the asymptotic approximation to the free boundary for the American put option. We present numerical experiments in order to study the accuracy and effectiveness of the 2D PDE and asymptotic approximations.

Key words: valuation adjustment; stochastic default; mean reversion process; free boundary; Black-Scholes PDE; asymptotic approximation

1 Introduction

American-type financial derivatives are widely traded on markets, and this makes the accurate and efficient pricing important. Credit valuation adjustment (CVA) and debt value adjustment (DVA) are the valuation adjustments to financial derivative prices due to the bilateral trading parties' default risks. Often, people use the total valuation adjustment (XVA) to refer to the sum of several different types of valuation adjustments. In this paper, we study modelling XVA pricing for American put options, numerical methods to approximate the free boundary of the linear complementarity problem arising and the price of XVA, under stochastic counterparty default intensity. Although we use American put option as an example, the ideas and techniques can be extended similarly to other financial derivatives.

Partial differential equations (PDEs) are often used to model option pricing, including XVA pricing. Monte Carlo simulation is another popular approach used in many research works. The PDE approach has several advantages: more accurate and reproducible valuation, faster convergence especially in low-dimensions, and more accurate and efficient computation of the so-called Greeks. In addition, the PDE formulation is easier to modify to make it suitable for American option pricing, because the exercise boundary is not easily obtained by Monte Carlo methods. The most obvious downside of PDE approach is that it suffers from the curse of dimensionality when the model has many (e.g five or more) spatial dimensions. The PDE formulation of bilateral XVA firstly appeared in Burgard and Kjaer's researches

[4, 5, 6, 7]. In their work, using the replication technique, and assuming constant default risks for both parties, a PDE model is derived to obtain the derivatives' value if CVA is considered. Compared to the vanilla Black-Scholes PDE, the XVA PDE involves a nonlinear source term. In [2, 3], the authors proposed PDEs for pricing European and American style options, respectively, with XVA, considering stochastic spreads. They use the finite element method for spatial discretization and the characteristic method for timestepping. They solve the nonlinear term arising from XVA by a fixed-point method, and the complementarity problem from American option constraints by the augmented Lagrangian active set method. In [8], the authors developed a double-penalty method to efficiently deal with the nonlinear terms arising from XVA and the linear complementarity constraints for American derivatives, assuming both counterparty default intensities are constant.

If we assume that the counterparty default risk intensities or other variables are stochastic, the spatial dimension of the problem is increased, which also increases the computation exponentially. In this paper, we assume that the default intensity of one counterparty is stochastic following mean-reversion, more specifically, a Cox-Ingersoll-Ross (CIR) process. This makes the counterparty default intensity λ_C a spatial variable in the PDE formulation, and results in a two-dimensional (2D) time-dependent nonlinear PDE problem, with a nonlinear term arising from the American constraint and another from XVA, the latter involving explicitly the variable λ_C. We extend the double-penalty method in [8] to the solution of the 2D PDE. We present algorithms for the accurate calculation of the free boundary for any λ_C.

Singular perturbation theory can be applied to multi-dimensional (e.g. 2D) PDEs to obtain approximations to their solution using lower-dimensional (e.g. 1D) PDEs and some correction terms, assuming certain functions, variables, or parameters have asymptotic expansions in terms of a small quantity. Such techniques are much more efficient than directly solving the multi-dimensional PDE. However, they are also challenging when linear complementarity PDE problems are to be solved, because the location of the boundary to the PDE region is unknown. In [12], the authors consider American options under fast mean-reversion volatility, and apply asymptotic expansion in terms of the mean-reversion speed for both the option price and the free boundary. As a result, the solution and free boundary of the 2D American problem are approximated by the solution and free boundary, respectively, of an 1D American problem plus appropriate correction terms. The authors claim that the asymptotic accuracy of the free boundary approximation is only order of half. In later work [1], additional correction terms are introduced and the approximation to the free boundary is slightly improved. In [16], the authors give a general presentation of singular perturbation theory and apply it to the Black-Scholes PDE assuming a small volatility, in terms of which the expansions are written. They use this technique to price vanilla European, American and Barrier options. In their American options asymptotic approximations, they also expand the value of the free boundary in terms of volatility, and come up with multiple correction terms added to the strike price.

We assume a fast mean-reverting λ_C, and develop an efficient approximation method similar to the one presented in [9], designed to work for American derivatives. The idea of dealing with the free boundary in this paper is similar to the one in [12, 1], but expansions are in terms of the mean reversion speed, and we use more expansion terms.

In this paper, we present the 2D PDE formulation of American XVA pricing assuming mean-reverting counterparty default intensity, numerical algorithms for computing the solution and free boundary, and an asymptotic approach for approximating the solution and free boundary using the solution of an 1D American XVA pricing problem and some correction terms. More specifically, the contributions of this work are

- We formulate a time-dependent PDE in two spatial dimensions, with multiple nonlinear source terms. One nonlinear term models the American constraint, and the other (which in turn consists of multiple

subterms) models the XVA adjustments.

- We extend the double-penalty method [8] to handle the different nonlinear source terms of the 2D PDE.
- We develop algorithms for the accurate approximation of the free boundary for any λ_C.
- We extend the asymptotic approximation we developed for European derivatives in [9] to American derivatives in the XVA pricing problem, and present algorithms to compute an asymptotic approximation to the free boundary, and an asymptotic approximation to the American XVA price. We study how the approximate free boundary affects our asymptotic approximated prices.
- We present numerical experiments to study the accuracy of the 2D PDE and asymptotic approximations, the effect of speed of mean-reversion to the adjusted prices and to the free boundary, and the behavior of the free boundary as the counterparty default intensity varies. We also compare the 2D PDE and asymptotic approximations.

The outline of this paper is as follows. In Section 2, we present the formulation of the American-type XVA pricing problem as a linear complementarity PDE. We also present the penalty form to the corresponding problem. In Section 3, we describe the numerical methods used for discretizations, the appropriate boundary conditions, the double-penalty method to deal with the multiple nonlinearities, and the algorithm for the accurate calculation of the free boundary. In Section 4, we present the asymptotic approximations to the free boundary and to the solution of the problem. In Section 5, numerical experiments' results are shown to compare the numerical PDE and asymptotic solutions for American put options, and to study their accuracy and effectiveness. Section 6 presents the conclusions and possible future works.

2 Formulation

In this section, we show the PDE formulation of the XVA pricing problem for American derivatives, with the stochastic counterparty default risk considered. The respective European XVA PDE model was developed in [9], using multiple hedging arguments, including underlying assets, the zero-coupon bonds of the two parties, risk-free zero-coupon bonds and another similar financial derivative; see also [11]. Similarly to the original American option PDE, the XVA pricing for American derivatives, when the stochastic counterparty default intensity is considered, is also a linear complementarity problem (LCP). In this paper, we assume that, if either party of a contract defaults, the Mark-to-Market value M is same as the value of the derivative including XVA, $\hat{V}$. We use the same notations as those in [9]: Let S be the underlying stock value, t the forward time, T the expiry time of the contract, σ the volatility in S, r the risk-free interest rate, γ the dividend yield of S, q the stock repo rate, λ_B the bank default intensity, λ_C the counterparty default intensity, R_B the recovery percentage on $M(=\hat{V})$ if seller defaults, R_C the recovery percentage on $M(=\hat{V})$ if counterparty defaults, r_F the seller's funding rate for borrowed cash, where $r_F = r + (1 - R_B)\lambda_B$ if derivative cannot be used as collateral, and $s_F = r_F - r$. The positive and negative values of any financial security W are denoted as $W^+ \equiv \max\{W, 0\}$ and $W^- \equiv \min\{W, 0\}$. Let also $r_R = q - \gamma$. Furthermore, let κ and θ be the rate and level of mean reversion, respectively, and σ^{λ_C} the CIR mean reversion process volatility.

When the backward time $\tau = T - t$ is applied, the American derivative price $\hat{V}(\tau, S, \lambda_C)$, taking stochastic risk into account, satisfies

$$\left\{ \begin{array}{r} \frac{\partial \hat{V}}{\partial \tau} - \mathcal{L}\hat{V} - f(\lambda_C, \hat{V}) > 0 \\ \hat{V} - V^* = 0 \end{array} \right\} \text{ or } \left\{ \begin{array}{r} \frac{\partial \hat{V}}{\partial \tau} - \mathcal{L}\hat{V} - f(\lambda_C, \hat{V}) = 0 \\ \hat{V} - V^* \geq 0 \end{array} \right\} \tag{1}$$

where

$$\mathcal{L}\hat{V} \equiv \frac{1}{2}(\sigma^S)^2 S^2 \frac{\partial^2 \hat{V}}{\partial S^2} + \frac{1}{2}(\sigma^{\lambda_C})^2 \lambda_C \frac{\partial^2 \hat{V}}{\partial \lambda_C^2} + \rho \sigma^S \sigma^{\lambda_C} S \sqrt{\lambda_C} \frac{\partial^2 \hat{V}}{\partial S \partial \lambda_C} + r_R S \frac{\partial \hat{V}}{\partial S} + \kappa[\theta - \lambda_C] \frac{\partial \hat{V}}{\partial \lambda_C} - r\hat{V}, \tag{2}$$

$$f(\lambda_C, \hat{V}) \equiv -(s_F + (1 - R_C)\lambda_C)\hat{V}^+ - (1 - R_B)\lambda_B \hat{V}^-, \tag{3}$$

$$V^* \equiv \hat{V}(0, S, \lambda_C). \tag{4}$$

Problem (1) is a free boundary problem, with the free boundary being a surface which can be written as $S_{fb}(\tau, \lambda_C)$. The free boundary separates the domain into two regions. We refer to the region where the left part of (1) holds as exercise or penalty region, and the region where the right part of (1) holds as hold or PDE region. Without loss of generality, we consider the American put case. In this case, in the hold region in (1), we have $S \geq S_{fb}$, while, in the exercise region, we have $S < S_{fb}$. We also have the initial condition

$$\hat{V}(0, S, \lambda_C) = (K - S)^+, \tag{5}$$

and the free boundary conditions

$$\hat{V}(\tau, S_{fb}, \lambda_C) = K - S_{fb}, \tag{6}$$

$$\frac{\partial \hat{V}}{\partial S}(\tau, S_{fb}, \lambda_C) = -1, \tag{7}$$

$$\frac{\partial \hat{V}}{\partial \lambda_C}(\tau, S_{fb}, \lambda_C) = 0. \tag{8}$$

2.1 Penalty formulation

For one-asset American option pricing without considering default risk, Forsyth and Vetzal [10] proposed the discrete penalty method to numerically solve the LCP. A large positive penalty term is added to the Black-Scholes equation, resulting in a nonlinear PDE. In [10], a rigorous study of equivalence between the LCP and the penalized nonlinear PDE is presented. In [8], the double-penalty method is firstly introduced to solve the LCP arising from American type XVA with constant bilateral default risk, which, in its penalty formulation, has multiple nonlinear terms.

In the current multi-dimensional American XVA problem, with stochastic counterparty default risk, a similar penalty term can be added. The penalty form of (1) is written as

$$\begin{cases} \frac{\partial \hat{V}}{\partial \tau} = \mathcal{L}\hat{V} + f(\lambda_C, \hat{V}) + p \max(V^* - \hat{V}, 0), \\ \hat{V}(0, S, \lambda_C) = (K - S)^+, \end{cases} \tag{9}$$

where p is a large positive penalty factor. The penalty term forces the solution of (9) to approximately satisfy the obstacle condition $\hat{V} - V^* \geq 0$.

2.2 Penalized-form PDE with constant default intensity

For later purposes, we give here the 1D American XVA LCP when the default intensity λ_C is given by a constant λ_C^c, formulated in [8],

$$\left\{ \begin{array}{r} \frac{\partial \hat{V}^c}{\partial \tau} - \mathcal{L}^c \hat{V}^c - f(\lambda_C^c, \hat{V}^c) > 0 \\ \hat{V}^c - V^* = 0 \end{array} \right\} \text{ or } \left\{ \begin{array}{r} \frac{\partial \hat{V}^c}{\partial \tau} - \mathcal{L}^c \hat{V}^c - f(\lambda_C^c, \hat{V}^c) = 0 \\ \hat{V}^c - V^* \geq 0 \end{array} \right\} \tag{10}$$

and the associated penalized PDE,

$$\frac{\partial \hat{V}^c}{\partial \tau} = \mathcal{L}^c \hat{V}^c + f(\lambda_C^c, \hat{V}^c) + p \max\{V^* - (\hat{V}^c)^-, 0\}, \tag{11}$$

where

$$\mathcal{L}^c \hat{V}^c \equiv \frac{1}{2}(\sigma^S)^2 S^2 \frac{\partial^2 \hat{V}^c}{\partial S^2} + r_R S \frac{\partial \hat{V}^c}{\partial S} - r\hat{V}^c. \tag{12}$$

Here, $\hat{V}^c$ is the adjusted American derivative price when taking constant default intensity λ_C^c into account, and the initial conditions are $\hat{V}^c(0, S) = (K - S)^+$. The LCP (10) has a free boundary $S_{fb}^c(\tau)$, satisfying the free boundary conditions

$$\hat{V}^c(\tau, S_{fb}^c) = K - S_{fb}^c, \tag{13}$$

$$\frac{\partial \hat{V}^c}{\partial S}(\tau, S_{fb}^c) = -1. \tag{14}$$

3 Numerical 2D PDE methods

3.1 Domain and discretization

The domain of PDE (9), which is the same that of the PDE problem (1), is semi-infinite in the two spatial variables: $(\tau, S, \lambda_C) \in (0, T] \times [0, \infty) \times [0, \infty)$. For computational purposes, the semi-infinite domains of S and λ_C are truncated, and we get the computational domain $(\tau, S, \lambda_C) \in (0, T] \times [0, S^{max}) \times [0, \lambda_C^{max})$, for sufficiently large S^{max} and λ_C^{max}. Then, $[0, S^{max}]$ and $[0, \lambda_C^{max}]$ are discretized with $S_0 = 0 < S_1 < \ldots < S_N = S^{max}$ and $(\lambda_C)_0 = 0 < (\lambda_C)_1 < \ldots < (\lambda_C)_M = \lambda_C^{max}$ the (uniform or nonuniform) gridpoints in the S and λ_C directions, respectively.

For the time domain, let $\tau_j, j = 0, \ldots, N_t$, with $\tau_0 = 0 < \tau_1 < \cdots < \tau_{N_t} = T$, denote the timesteps at which the solution is computed. If uniform timesteps are used, then $\Delta\tau = T/N_t$ is the time stepsize, otherwise, let $\Delta\tau^j = \tau_j - \tau_{j-1}$.

The space discretization of the PDE (1) uses techniques similar to [9], except that the penalty term needs to be taken into account. All interior points are discretized by second-order centered differences, while boundary points by one-sided differences.

For the boundary and corner equations, we again use similar treatment as in [9], with the addition of the penalty term $p \max(V^* - \hat{V}, 0)$. Omitting the details for brevity, we give one example how the penalty term is introduced. On $\{(S, \lambda_C) \in \{S = 0\} \times [0, \lambda_C^{max}]\}$, set $S = 0$ in (9), and, instead of Equation (44) in [9], obtain

$$\frac{\partial \hat{V}}{\partial \tau} = \frac{1}{2}(\sigma^{\lambda_C})^2 \lambda_C \frac{\partial^2 \hat{V}}{\partial \lambda_C^2} + \kappa[\theta - \lambda_C] \frac{\partial \hat{V}}{\partial \lambda_C} - r\hat{V} + f(\lambda_C, \hat{V}) + p \max(V^* - \hat{V}, 0), \tag{15}$$

which, with $\lambda_C = 0$ on the left, and linear boundary condition $\frac{\partial^2 \hat{V}}{\partial \lambda_C^2} = 0$ on the right, is numerically solved as an 1D parabolic PDE, giving Dirichlet boundary conditions for (9) on $S = 0$.

Note that the boundary conditions on $\{(S, \lambda_C) \in \{S = 0\} \times [0, \lambda_C^{max}]\}$ are solved separately, while the boundary conditions on $\{(S, \lambda_C) \in \{S = S^{max}\} \times [0, \lambda_C^{max}]\}$, $\{(S, \lambda_C) \in (0, S^{max}) \times \{\lambda_C = 0\}\}$, and $\{(S, \lambda_C) \in (0, S^{max}) \times \{\lambda_C = \lambda_C^{max}\}\}$ form part of the $N(M+1) \times N(M+1)$ linear system solved

at each timestep. In [9], there is more detailed discussion on the European boundary conditions including corners as well as the discretization of the conditions.

We use the ϑ-method [†], in its Crank-Nicolson-Rannacher formulation, for time-stepping, that is, apply four half-timesteps of Backward Euler (BE $\vartheta = 1$), then continue with the remaining $N_t - 2$ (full) timesteps as Crank-Nicolson (CN, $\vartheta = \frac{1}{2}$).

3.2 Penalty discretization and double-penalty iteration

In this subsection, we briefly present the discretization of the nonlinear terms $p\max(V^* - \hat{V}, 0)$ (arising from the early-exercise of American options) and $f(\lambda_C, \hat{V})$ (arising from the XVA, with stochastic λ_C), and the algorithm used for the solution at each timestep. Let $\hat{v}^j, j = 0, \ldots, N_t$, be the computed solution vector at time τ_j, $\hat{v}^0$ be the initial condition vector, and v^* be the vector of values of payoff V^*, all vectors with components along the spatial gridpoints in a bottom-up (λ_C direction) then left-to-right (S direction) ordering.

Because there are similarities between the method used here and the method in [8], as well as between some matrices used here and in [9], rather than repeating the material in [8] and [9], we refer to some relations in [8, 9], and emphasize on the differences.

The nonlinear term $p\max(V^* - \hat{V}, 0)$ is discretized as $P_A(\hat{v}^j)(v^* - \hat{v}^j)$, where $P_A(\hat{v}^j)$ is a diagonal matrix defined as in Equation (4.9) in [8]. However, there are differences between the P_A of [8], and the P_A used here. The P_A matrix of [8] is a diagonal matrix with "p"s followed by zeroes along the diagonal. The P_A matrix here is also diagonal, but should be viewed as a block-diagonal matrix with diagonal blocks, with the nonzero components not concentrated towards the top-left, but rather "block-concentrated" towards the top-left of *each block*, and the zeroes towards the bottom-right of *each block*.

The nonlinear term $f(\lambda_C, \hat{V})$ is discretized as $P_X(\hat{v}^j)(\hat{v}^j)$, where $P_X(\hat{v}^j)$ is a diagonal matrix defined as matrix P in Equation (54) in [9].

Once we have the P_A and P_X matrices defined, and assuming A is the matrix arising from the space discretization of $\mathcal{L}\hat{V}$ (two-dimensional), and $\mathbb{I}$ the identity matrix of compatible order, we need to solve the system of algebraic equations given by Equation (4.11) in [8]. This system is solved by the discrete double-penalty iteration given as Algorithm 3 in [8], with the stopping criterion given by Equation (4.12) in [8].

We emphasize that the two nonlinear terms are updated simultaneously, and not in a nested way. The sparsity structure of the matrix solved at each iteration is block-tridiagonal, just as A is. Note that, as in [9], the diagonal of A is enhanced by P_X, under typical conditions. Also, since $p > 0$, the diagonal of $\mathbb{I} - \vartheta\Delta\tau^j(A + P_X^{j,k-1})$ is enhanced by P_A.

3.3 Numerical approximation of free boundary of multi-dimensional American XVA problem

In this subsection, we show how to numerically approximate the free boundary of the multi-dimensional American XVA problem on a specific desired λ_C point, assuming we already have numerical solutions on the grid points, $(S_i, (\lambda_C)_j), i = 1, \ldots, N, j = 0, \ldots, M$.

The naive way is that, for a fixed λ_C, we choose the free boundary point as the point S_k to the left of the first grid point S_{k+1}, where the numerical solution is a certain tolerance, e.g. $2tol = \frac{2}{p}$, or more above the payoff function. Following this naive way, S_k maybe different for each λ_C, but it is always chosen among the grid points S_i, $i = 1, \ldots, N$.

[†]Note that the ϑ notation for the time-stepping method is different from the $\theta(t)$ notation in the CIR model

The above approximation is improved in accuracy following [15]. Along each λ_C line, for which we want to approximate the free boundary, we construct an interpolant $V_\partial(S)$ of the first (with respect to S) derivative values and find for which S it satisfies $V_\partial(S) = -1$. The interpolant is constructed using three points $\{(S_i, \frac{\partial \hat{V}}{\partial S}(S_i, \lambda_C)), i = k+1, k+2, k+3\}$ away from the naive free boundary S_k and in the PDE region (hold region), as the error on S_k is contaminated with errors from the early exercise region that are not smooth, and the finite difference approximations involving S_k are inaccurate. See Algorithm 1 for details. To solve the nonlinear equation $V_\partial(S) + 1 = 0$ we can use the standard quadratic root formula or Newton's method with initial guess S_{k+1}. An alternative is to construct a quadratic interpolant $V_I(S)$ of $\hat{V}(S)$ using $\{(S_i, \hat{V}(S_i), \lambda_C), i = k+1, k+2, k+3\}$, and to solve $V_I(S) - V^*(S) = 0$ for S. This nonlinear equation has a double root, so Newton's method is expected to be slow. But the quadratic formula could still work well. In our code, we used the MATLAB function `fsolve` on $V_\partial(S) + 1 = 0$ with initial guess S_{k+1}, and tolerance 10^{-9}.

In Algorithm 1, we assume we have already computed numerical approximations to $\hat{V}(S_i, (\lambda_C)_j)$, $i = 1, 2, \ldots, N, j = 0, 1, \ldots, M$. For simplicity, we denote the approximations by $\hat{V}(S_i, (\lambda_C)_j)$ as well. Furthermore, we note that Algorithm 1 works even if the given λ_C is not a gridpoint; see Step 1 of Algorithm 1. We also note that the FD approximation to $\frac{\partial \hat{V}}{\partial S}(S_{k+1})$ in Step 4 is one-sided, to avoid using points into the exercise region.

Algorithm 1 American XVA 2D PDE: Approximation of the free boundary for a given λ_C.

1: If λ_C is not a grid point, compute approximations $\hat{\hat{V}}(S_i, \lambda_C)$ to $\hat{V}(S_i, \lambda_C), i = 1, 2, \ldots, N$, by cubic spline interpolation on the values $\hat{V}(S_i, (\lambda_C)_j)$, $i = 1, 2, \ldots, N, j = 0, 1, \ldots, M$. Let $\hat{V}(S_i) = \hat{\hat{V}}(S_i, \lambda_C)$, $i = 1, 2, \ldots, N$.
2: If λ_C is grid point $(\lambda_C)_j$, let $\hat{V}(S_i) = \hat{V}(S_i, (\lambda_C)_j)$, $i = 1, 2, \ldots, N$.
3: Find the leftmost point S_{k+1}, such that $\hat{V}(S_{k+1}) - V^*(S_{k+1}) \geq 2tol$.
4: Compute finite difference approximations $\frac{\partial \hat{V}}{\partial S}(S_i)$, to $\frac{\partial \hat{V}}{\partial S}(S_i, \lambda_C), i = k+1, k+2, k+3$.
5: Construct the quadratic interpolant $V_\partial(S)$ of $\frac{\partial \hat{V}(S)}{\partial S}$ using $\{(S_i, \frac{\partial \hat{V}}{\partial S}(S_i)), i = k+1, k+2, k+3\}$.
6: Solve $V_\partial(S) + 1 = 0$ for S with initial guess S_{k+1}, to get the free boundary $S_{fb}^{\lambda_C}$ for the given λ_C.

4 Asymptotic methods

Numerically solving the time-dependent multi-dimensional PDE, especially including multiple nonlinear source terms, is computationally expensive. An asymptotic approximation can ease this problem [11, 9, 14]. An asymptotic approximation requires the solution of a lower-dimensional PDE and applies some correction terms to it by a closed-form formula. However, asymptotic approximation for path-dependent derivatives is more complicated due to the lack of explicit formula for the corrections terms. For example, for American put, this problem is more involved due to the singularities at the free boundaries, because, usually at the free boundary points, the solutions are only $\mathbb{C}^1$. In [12, 1], the authors applied asymptotic expansions to both the value function and the free boundary and find an asymptotic correction to the free boundary, which transforms the two-dimensional free boundary problem into a fixed boundary problem.

The stochastic differential equation that the CIR process for λ_C follows is the same as given by Equation (59) in [9]. Following [13, 14, 8, 9], we assume $\kappa = 1/\epsilon$, where $\epsilon > 0$ is small. We also scale σ^{λ_C}

as $\sigma^{\lambda_C} = \frac{\nu}{\sqrt{\epsilon}}$, to keep ν^2 constant as ϵ becomes smaller. Hence we can rewrite the equation in the hold region of (1) as

$$(\frac{1}{\epsilon}\mathcal{L}_0 + \frac{1}{\sqrt{\epsilon}}\mathcal{L}_1 + \mathcal{L}_2)\hat{V} = 0, \tag{16}$$

where

$$\mathcal{L}_0 \equiv \frac{1}{2}\nu^2\lambda_C\frac{\partial^2}{\partial\lambda_C^2} + (\theta - \lambda_C)\frac{\partial}{\partial\lambda_C}, \tag{17}$$

$$\mathcal{L}_1 \equiv \rho\sigma^S\nu S\sqrt{\lambda_C}\frac{\partial^2}{\partial S\partial\lambda_C}, \tag{18}$$

$$\mathcal{L}_2 \equiv (-\frac{\partial}{\partial\tau}) + \frac{1}{2}(\sigma^S)^2S^2\frac{\partial^2}{\partial S^2} + r_R S\frac{\partial}{\partial S} - r\mathcal{I} + f(\lambda_C, \hat{V}), \tag{19}$$

with $\mathcal{I}$ being the identity operator.

4.1 Asymptotic expansions

We apply asymptotic expansion to both $\hat{V}$ and S_{fb} with respect to ϵ,

$$\hat{V} \equiv \hat{V}^\epsilon = \hat{V}_0 + \sqrt{\epsilon}\hat{V}_{1/2}{}^\ddagger + \epsilon\hat{V}_1 + \epsilon\sqrt{\epsilon}\hat{V}_{3/2} + \ldots, \tag{20}$$

$$S_{fb} \equiv S_{fb}^\epsilon = S_{f0} + \sqrt{\epsilon}S_{f1/2} + \epsilon S_{f1} + \ldots, \tag{21}$$

which converge to the exact respective solutions if $\epsilon \to 0$. In this paper, we use the first three terms of (20) to estimate $\hat{V}$, such that $\hat{V} \approx \hat{V}^{\epsilon,1} \equiv \hat{V}_0 + \sqrt{\epsilon}\hat{V}_{1/2} + \epsilon\hat{V}_1$, and the first two terms of (21) to estimate the free boundary S_{fb}, such that $S_{fb} \approx S_{fb}^{\epsilon,1/2} \equiv S_{f0} + \sqrt{\epsilon}S_{f1/2}$.

In the following, we derive formulae for computing $\hat{V}_0$, $\hat{V}_{1/2}$, $\hat{V}_1$, S_{f0} and $S_{f1/2}$. Let $\langle\cdot\rangle$ denote expectation with respect to the invariant distribution of λ_C.
The expansion of the partial differential equation (16) (hold region) gives

$$\mathcal{O}(\frac{1}{\epsilon}) : \mathcal{L}_0\hat{V}_0 = 0 \tag{22}$$

$$\mathcal{O}(\frac{1}{\sqrt{\epsilon}}) : \mathcal{L}_0\hat{V}_{1/2} + \mathcal{L}_1\hat{V}_0 = 0 \tag{23}$$

$$\mathcal{O}(1) : \mathcal{L}_0\hat{V}_1 + \mathcal{L}_1\hat{V}_{1/2} + \mathcal{L}_2\hat{V}_0 = 0 \tag{24}$$

$$\mathcal{O}(\sqrt{\epsilon}) : \mathcal{L}_0\hat{V}_{3/2} + \mathcal{L}_1\hat{V}_1 + \mathcal{L}_2\hat{V}_{1/2} = 0. \tag{25}$$

We also expand the free boundary conditions (6), (7) and (8), keeping terms up to $\sqrt{\epsilon}$, as

$$\hat{V}_0(S_{f0}) + \sqrt{\epsilon}(S_{f1/2}\frac{\partial\hat{V}_0}{\partial S}(S_{f0}) + \hat{V}_{1/2}(S_{f0})) = K - S_{f0} - \sqrt{\epsilon}S_{f1/2}, \tag{26}$$

$$\frac{\partial\hat{V}_0}{\partial S}(S_{f0}) + \sqrt{\epsilon}(S_{f1/2}\frac{\partial^2\hat{V}_0}{\partial S^2}(S_{f0}) + \frac{\partial\hat{V}_{1/2}}{\partial S}(S_{f0})) = -1, \tag{27}$$

$$\frac{\partial\hat{V}_0}{\partial\lambda_C}(S_{f0}) + \sqrt{\epsilon}(S_{f1/2}\frac{\partial^2\hat{V}_0}{\partial S\partial\lambda_C}(S_{f0}) + \frac{\partial\hat{V}_{1/2}}{\partial\lambda_C}(S_{f0})) = 0, \tag{28}$$

‡In the notations $\hat{V}_{1/2}$, $S_{1/2}$ and $\hat{V}_{3/2}$, the subscripts are consistent with the powers of the associated ϵ coefficients.

where, for brevity, though all quantities are at $(\tau, S_{f0}, \lambda_C)$, we omit τ and λ_C. From Equations (26)–(28), we have

$$\hat{V}_0(S_{f0}) = K - S_{f0}, \tag{29}$$

$$\frac{\partial \hat{V}_0}{\partial S}(S_{f0}) = -1, \tag{30}$$

$$\frac{\partial \hat{V}_0}{\partial \lambda_C}(S_{f0}) = 0, \tag{31}$$

$$S_{f1/2}\frac{\partial^2 \hat{V}_0}{\partial S^2}(S_{f0}) + \frac{\partial \hat{V}_{1/2}}{\partial S}(S_{f0}) = 0. \tag{32}$$

In the exercise region, the condition $\hat{V} = (K-S)^+$ suggests that $\hat{V}_0 = (K-S)^+$, $\hat{V}_{1/2} = 0$ and $\hat{V}_1 = 0$.

Since we have (22) in the hold and $\hat{V}_0 = (K-S)^+$ in the exercise regions, $\hat{V}_0$ is independent of λ_C in both regions, i.e. $\hat{V}_0 = \hat{V}_0(\tau, S)$. This implies $\mathcal{L}_1\hat{V}_0 = 0$. Then, in the hold region, Equation (23) results in $\mathcal{L}_0\hat{V}_{1/2} = 0$, which, together with $\hat{V}_{1/2} = 0$ in the exercise region, imply $\hat{V}_{1/2}$ is independent of λ_C as well in both regions. i.e. $\hat{V}_{1/2} = \hat{V}_{1/2}(\tau, S)$. This also results in $\mathcal{L}_1\hat{V}_{1/2} = 0$ in the hold region.

In the hold region, since $\mathcal{L}_1\hat{V}_{1/2} = 0$, Equation (24), reduces to $\mathcal{L}_0\hat{V}_1 + \mathcal{L}_2\hat{V}_0 = 0$, which, as a Poisson equation with respect to $\mathcal{L}_0$ in λ_C, results in $\langle\mathcal{L}_2\rangle\hat{V}_0 = 0$, which, in turn, is the PDE in the hold region of LCP (10), with $\lambda_C^c = \theta$. In addition, Equations (29)-(30) indicate that S_{f0} satisfies the free boundary conditions (13)-(14) for this LCP. In the exercise region, we have $\hat{V}_0 = (K-S)^+$. Therefore, $\hat{V}_0$ is the solution to the 1D American Black-Scholes XVA problem with constant default intensity being the mean of the CIR model, that is, LCP (10), with $\lambda_C^c = \theta$, and S_{f0} is the free boundary of the LCP. To compute the solution to this problem, no analytical formula is available. An advanced numerical method, such as a penalty method, can be used to approximate the corresponding 1D penalized PDE (11) with terminal condition $\hat{V}_0(0, S) = (K-S)^+$.

As in [9], from (25), we get $\langle\mathcal{L}_2\rangle\hat{V}_{1/2} = -\langle\mathcal{L}_1\hat{V}_1\rangle$. Using $\mathcal{L}_0\hat{V}_1 = -\mathcal{L}_2\hat{V}_0$, $\langle\mathcal{L}_2\rangle\hat{V}_{1/2} = -\langle\mathcal{L}_1\hat{V}_1\rangle$, and techniques similar to [9], we can obtain the solution to $\hat{V}_1$ in terms of $\hat{V}_0$. Likewise, we can obtain the solution to $\hat{V}_{1/2}$ in terms of $\hat{V}_0$. The formulae are as in [9],

$$\hat{V}_{1/2}(\tau, S) = -\tau\rho\sigma^S\nu S(1-R_C)\langle\sqrt{\lambda_C}\rangle\frac{\partial \hat{V}_0^+}{\partial S}, \tag{33}$$

$$\hat{V}_1(\tau, S, \lambda_C) = (1-R_C)(\theta - \lambda_C)\hat{V}_0^+ + \tau(1-R_C)^2\frac{\theta\nu^2}{2}\hat{V}_0^+, \tag{34}$$

but notice that, here, $\hat{V}_0$ is the solution to the 1D American Black-Scholes XVA problem with constant default intensity $\lambda_C^c = \theta$. Note that the approximation $\hat{V} \approx \hat{V}^{\epsilon,1}$ (with $\hat{V}_{1/2}$ as in (33) and $\hat{V}_1$ as in (34)) is only for the hold region, while, in the exercise region, we have $\hat{V} = V^*$. From (32) and (33), we also have the correction to the free boundary

$$S_{f1/2} = \left.\frac{-\frac{\partial \hat{V}_{1/2}}{\partial S}}{\frac{\partial^2 \hat{V}_0}{\partial S^2}}\right|_{S=S_{f0}} = \left.\frac{\tau\rho\sigma^S\nu(1-R_C)\langle\sqrt{\lambda_C}\rangle(\frac{\partial \hat{V}_0^+}{\partial S} + S\frac{\partial^2 \hat{V}_0^+}{\partial S^2})}{\frac{\partial^2 \hat{V}_0}{\partial S^2}}\right|_{S=S_{f0}}. \tag{35}$$

From the view of computation, given $\hat{V}_0$, S_{f0} is computed in a way similar to Algorithm 1, but adjusted to work on the 1D problem. See steps 1–4 of Algorithm 2.

Note that, for Equations (33) and (35), we define

$$\frac{\partial \hat{V}_0^+}{\partial S} \equiv \begin{cases} \frac{\partial \hat{V}_0}{\partial S} & \hat{V}_0 > 0 \\ 0 & \hat{V}_0 \leq 0 \end{cases} \quad \text{and} \quad \frac{\partial^2 \hat{V}_0^+}{\partial S^2} \equiv \begin{cases} \frac{\partial^2 \hat{V}_0}{\partial S^2} & \hat{V}_0 > 0 \\ 0 & \hat{V}_0 \leq 0 \end{cases}, \tag{36}$$

and, in Equation (35), the partial derivatives at $S = S_{f0}$ are taken to be one-sided derivatives into the hold region; see Algorithm 2.

In the following, we describe the algorithm we apply for the approximation of S_{f0} and of the derivative values $\frac{\partial \hat{V}_0}{\partial S}(S_{f0})$, and $\frac{\partial^2 \hat{V}_0}{\partial S^2}(S_{f0})$, that are needed in (35). In Algorithm 2, we assume we have already computed numerical approximations to $\hat{V}_0(S_i)$, $i = 1, 2, \ldots, N$. For simplicity, we denote the approximations by $\hat{V}_0(S_i)$ as well.

Algorithm 2 American XVA PDE: Approximation of S_{f0} (steps 1–4), $\frac{\partial \hat{V}_0^+}{\partial S}(S_{f0})$ (step 5), and $\frac{\partial^2 \hat{V}_0}{\partial S^2}(S_{f0})$ and $\frac{\partial^2 \hat{V}_0^+}{\partial S^2}(S_{f0})$ (steps 6–8).

1: Find the leftmost point S_{k+1}, such that $\hat{V}_0(S_{k+1}) - V^*(S_{k+1}) \geq 2tol$.
2: Compute finite difference approximations to $\frac{\partial \hat{V}_0}{\partial S}(S_i), i = k+1, k+2, k+3$.
3: Construct the quadratic interpolant $V_{\partial,0}(S)$ of $\frac{\partial \hat{V}_0(S)}{\partial S}$ using $\{(S_i, \frac{\partial \hat{V}_0}{\partial S}(S_i)), i = k+1, k+2, k+3\}$.
4: Solve $V_{\partial,0}(S) + 1 = 0$ for S with initial guess S_{k+1}, to get the free boundary S_{f0}.
5: Set $\frac{\partial \hat{V}_0}{\partial S}(S_{f0}) = -1$; set $\frac{\partial \hat{V}_0^+}{\partial S}(S_{f0})$ as in (36).
6: Compute finite difference approximations to $\frac{\partial^2 \hat{V}_0}{\partial S^2}(S_i), i = k+1, k+2, k+3$.
7: Construct the quadratic interpolant $V_{\partial\partial,0}(S)$ of $\frac{\partial^2 \hat{V}_0(S)}{\partial S^2}$ using $\{(S_i, \frac{\partial^2 \hat{V}_0}{\partial S^2}(S_i)), i = k+1, k+2, k+3\}$.
8: Evaluate $V_{\partial\partial,0}(S_{f0})$ and set $\frac{\partial^2 \hat{V}_0}{\partial S^2}(S_{f0}) = V_{\partial\partial,0}(S_{f0})$; set $\frac{\partial^2 \hat{V}_0^+}{\partial S^2}(S_{f0})$ as in (36).

It is important to note that the interpolants $V_{\partial,0}(S)$ and $V_{\partial\partial,0}(S)$ are constructed using values into the hold region (where sufficient smoothness holds) and away from the penalty region, and that the approximations to $\frac{\partial \hat{V}_0}{\partial S}(S_{f0})$ and $\frac{\partial^2 \hat{V}_0}{\partial S^2}(S_{f0})$ are constructed using extrapolation of the interpolants.

To conclude, given a certain point, our asymptotic approximation to the American put option value including XVA, with stochastic default intensity, is summarized in Algorithm 3.

Algorithm 3 American XVA PDE: Asymptotic approximation to the free boundary and to the put option value at a given point S_{spot}

1: Compute $\hat{V}_0$, by numerically solving the 1D American put option XVA PDE (11), with $\lambda_C^c = \theta$, using the double-penalty method in [8].
2: Compute $\hat{V}_0^+$, $\frac{\partial \hat{V}_0}{\partial S}$ and $\frac{\partial \hat{V}_0^+}{\partial S}$ at S_{spot}, using $\hat{V}_0$, finite differences and (36).
3: Compute S_{f0}, $\frac{\partial \hat{V}_0^+}{\partial S}(S_{f0})$, $\frac{\partial^2 \hat{V}_0}{\partial S^2}(S_{f0})$, and $\frac{\partial^2 \hat{V}_0^+}{\partial S^2}(S_{f0})$, using $\hat{V}_0$ and Algorithm 2.
4: Compute correction terms $\hat{V}_{1/2}$ and $\hat{V}_1$ at S_{spot}, by Equations (33) and (34), respectively.
5: Compute correction term $S_{f1/2}$ to free boundary, by Equation (35).
6: Obtain the free boundary approximation $S_{fb}^{\epsilon,1/2} = S_{f0} + \sqrt{\epsilon} S_{f1/2}$.
7: **if** $S_{spot} \geq S_{fb}^{\epsilon,1/2}$ **then**
8: $\quad \hat{V} \approx \hat{V}^{\epsilon,1} = \hat{V}_0 + \sqrt{\epsilon}\hat{V}_{1/2} + \epsilon \hat{V}_1$.
9: **else**
10: $\quad \hat{V} \approx V^*$ (payoff function)
11: **end if**

REMARK 1 *Similarly as in [12], the basic strategy for constructing an asymptotic approximation is to asymptotically expand both the value $\hat{V}$ and the free boundary S_{fb} in terms of ϵ, and obtain an approximated free boundary. Then, using the approximated free boundary, we divide the spot price region into the hold and exercise region, and apply a different formula for the price at each region. However, the approximated free boundary is $O(\epsilon)$ from the true free boundary S_{fb}. Hence, when the spot price S is close to the exercise boundary, the contract might move to the exercise region, in which case, the derivatives do not exist long enough for the mean-reverting effects of fast mean-reverting stochastic counterparty default intensity. In this case, the asymptotic approximation is not expected to be accurate. This technique is more effective when it is applied to approximate the value away from the approximated free boundary $S_{fb}^{\epsilon,1/2}$.*

5 Numerical experiments

In this section, we show results of numerical experiments from applying the proposed methods on American put options. Table 1 presents the values of parameters we used in the experiments.

Parameter	Value
Domain of S	$[0, 8K]$
Domain of λ_C	$[0, 6.05]$
Strike Price, K	15
Time to maturity, T	1
Volatility of asset, σ^S	0.4
Volatility of intensity of party C, σ^{λ_C}	0.2
Correlation between S and λ_C, ρ	0.3
Mean reversion level of intensity of party C, θ	0.05
Mean reversion rate of intensity of party C, κ	1
Repo rate minus dividend, $r_R = q - \gamma$	0.015
Interest rate, r	0.03
Default intensity of party B, λ_B	0.02
Recovery rate of party B, R_B	0.4
Recovery rate of party C, R_C	0.3
Funding spread, s_F	$(1 - R_B)\lambda_B$

Table 1: Model parameters for bilateral XVA with stochastic default intensity in American put options.

5.1 Numerical PDE with double-penalty iterations

The spatial domain of (S, λ_C), $[0, S_{max}] \times [0, \lambda_C^{max}]$, is discretized into $N \times M$ subintervals. We choose the truncated boundaries, $S_{max} = 8K$ and $\lambda_C^{max} = 6.05$, when $\sigma^{\lambda_C} = 0.2$, as suggested in [9]. More generally, $\lambda_C^{max} = \theta + 30\sigma^{\lambda_C}$. In [9], the effect of truncated boundaries is studied in details for European options. We do not expect different behavior for American options, as far as truncated boundaries are concerned. We also choose to use nonuniform gridpoints on both S dimension and λ_C dimension. The gridpoints on S are concentrated around the strike price K, while the gridpoints on λ_C are concentrated towards 0. The formulae of the nonuniform mappings from uniform grids on these two spatial dimensions can be found in [9].

The spatial derivatives are discretized by standard second-order centered differences, except the first derivatives in the boundary conditions, which are discretized by first-order forward or backward differences. The number of timesteps in denoted by N_t, and $\Delta t = T/N_t$, as defined in Section 3. As explained in Section 3, the timestepping scheme is Crank-Nicolson-Rannacher. Algorithm 3 in [8], with the matrices as described in Section 3.2 in this paper, is used at each timestep. In all tables in this section, "iter tot" and "iter avg" mean total and average (per timestep) number of iterations. The tolerance tol of double-penalty iteration is set to 10^{-7}, thus $p = 10^7$.

We present results from pricing the XVA of American put options with stochastic counterparty default intensity, and with the parameter settings in Table 1. For American put options, the XVA with stochastic counterparty default intensity does not have an analytical solution. The error at one resolution is estimated by the difference from the previous (coarser) resolution. In Table 2, we show the results at-the-money with different resolutions. We notice that the average number of double-penalty iterations is around 2, and varies very little with grid size. The numerical results do not exhibit any instability, and the order of convergence is 2, which is the same as the theoretically expected convergence. In Table 3, we also list numerical results for several spot prices and different levels of default risk. In this problem with $K = 15$, asset price $S = 7.5$ is expected to be in the exercise region, while asset prices $S = 15$ and $S = 30$ are expected to be in the hold region. From Tables 2 and 3, we notice that when the underlying asset prices $S = 15$ and $S = 30$, the order of convergence is approximately 2 as expected. From Table 3, at $S = 7.5$,

the numerical solution converges quickly to 7.5, and this is because the errors in the exercise region are related to $\frac{1}{p} = 10^{-7}$ and less affected by the discretization size. Therefore, for high resolutions, the errors are beyond the seven digits, and calculating the order of convergence makes no sense.

We are also interested in the behavior of the free boundaries for different counterparty default intensities λ_C. In Table 4, we show the location and convergence of the free boundaries when $\lambda_C = 0.0615927$ and $\lambda_C = 0.1364300$ for the double-penalty method for several grid sizes. These λ_C points are chosen because they are grid points of all λ_C-grids from the coarsest to the finest. We could have picked other arbitrary λ_C points, but in such case, we need to apply interpolation to the computed values on the grid points to obtain the values at the arbitrary λ_C points, a procedure that may increase the errors. From Table 4, we notice that although the order of convergence of the free boundaries of the double-penalty method is not very stable, the changes from coarse to fine grids generally decrease and go down to levels of about 10^{-3}. In Table 5, we show the values of the free boundaries for several different λ_C that are not gridpoints. It is clear that, as the λ_C value increases, the free boundary value also increases, which means that the American derivative will be exercised for a larger range of S values. Usually, large counterparty default intensity results in valuation reduction in adjusted price. With the "push-up" effect of the payoff constraints from American put options, the free boundary should move to the right in the S-dimension.

We also investigate how the free boundary location changes with varying κ. Here, we assume that, as κ changes, σ^{λ_C} also changes, so that ν remains constant, i.e. $\sigma^{\lambda_C} = \nu\sqrt{\kappa}$. This scaling is the same as the one assumed in [9], and helps obtain results comparable to those obtained from the asymptotic approximation. Figure 1 plots the values of the free boundaries, versus counterparty default intensity λ_C, with various κ. From Figure 1, we again see that the free boundary increases with increasing default intensities λ_C. We also notice, from Figure 1, that the free boundaries are less sensitive with respect to κ around $\lambda_C = 0.05$, which is the long-run mean of mean-reversion process. When λ_C is smaller, the free boundaries increase with increasing κ, while, when λ_C is large, the free boundaries decrease with increasing κ.

N	M	N_t	iter tot	iter avg	$\hat{V}$ value for put option		
					value	diff in $\hat{V}$	order
16	8	10	19	1.90	2.1254085	–	–
32	16	18	33	1.83	2.1619127	3.65e-02	–
64	32	34	72	2.12	2.1714040	9.49e-03	1.94
128	64	66	149	2.26	2.1741303	2.73e-03	1.80
256	128	130	310	2.38	2.1748854	7.55e-04	1.85
512	256	258	678	2.63	2.1750101	1.25e-04	2.60
Richardson extrapolated value: 2.1750516							

Table 2: Results from solving (9) for American put option including bilateral XVA with stochastic default intensity on counterparty using Algorithm 3 in [8] with the parameters in Table 1 when S is at-the-money ($S = K = 15$) and $\lambda_C = \theta$. Nonuniform grids are used.

N, M, N_t	(7.5, 0.025)	(7.5, 0.05)	(7.5, 0.1)	(30, 0.025)	(30, 0.05)	(30, 0.1)
128, 66, 68	7.4999991	7.4999954	7.5000017	0.1224851	0.1213862	0.1191487
256,128,130	7.5000007	7.4999998	7.5000000	0.1227464	0.1216452	0.1194031
512,256,258	7.5000000	7.5000000	7.5000000	0.1227959	0.1216946	0.1194522
order	—-	—-	—-	2.40	2.39	2.37

Table 3: Results at various points (S, λ_C) from solving (9) for American put option including bilateral XVA with stochastic default intensity on counterparty using Algorithm 3 in [8] with the parameters in Table 1. Nonuniform grids are used.

N	FB at $\lambda_C = 0.0615927$			FB at $\lambda_C = 0.1364300$		
	value	diff	order	value	diff	order
16	7.7115593	–	–	7.8072792	–	–
32	8.2664888	5.55e-01	–	8.5645010	7.57e-01	–
64	8.3707357	1.04e-01	2.41	8.7553107	1.91e-01	1.99
128	8.4228745	5.21e-02	1.00	8.8585797	1.03e-01	0.89
256	8.4436199	2.07e-02	1.33	8.8946672	3.61e-02	1.52
512	8.4494439	5.82e-03	1.83	8.9049210	1.03e-02	1.82

Table 4: Free boundary locations and orders of convergence for various counterparty default intensity λ_C-points from solving (9) for American put option including bilateral XVA with stochastic default intensity on counterparty using Algorithm 3 in [8] with the parameters in Table 1. Nonuniform grids are used. Algorithm 1 is used for the calculation of free boundaries.

λ_C	0.01	0.025	0.05	0.1	0.2
FB	8.0060641	8.1536824	8.3647338	8.7032745	9.1982301

Table 5: Free boundary locations for various counterparty default intensity λ_C-points from solving (9) for American put option including bilateral XVA with stochastic default intensity on counterparty using Algorithm 3 in [8] with the parameters in Table 1. Nonuniform grids are used and $N = 512$. Algorithm 1 is used for the calculation of free boundaries.

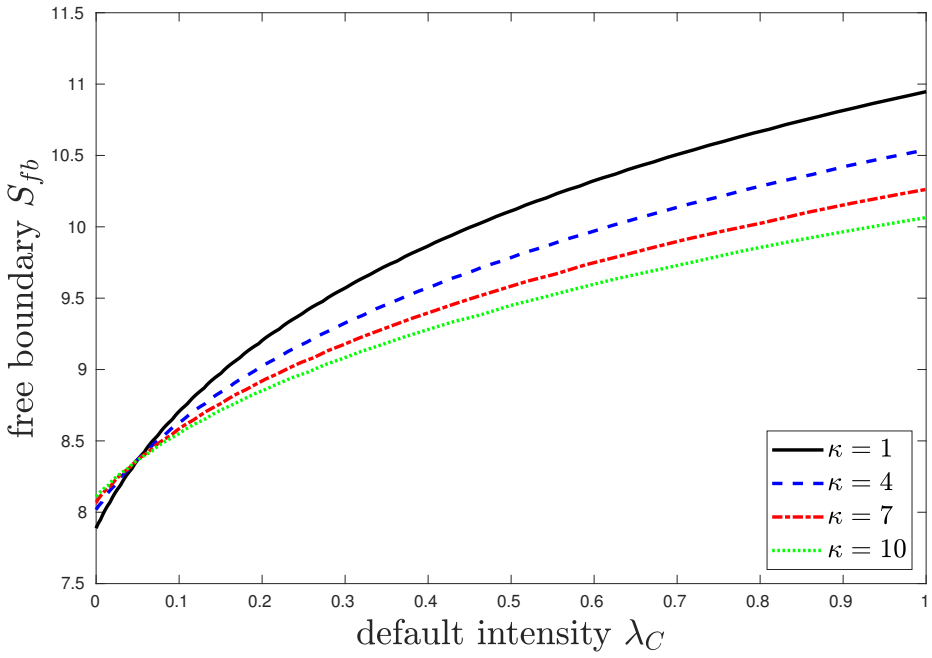

Figure 1: Free boundary locations versus the counterparty default intensity λ_C, with various mean-reversion speeds κ from solving (9) for American put option including bilateral XVA with stochastic default intensity on counterparty using Algorithm 3 in [8] with the parameters in Table 1. Nonuniform grids are used and $N = 512$. Algorithm 1 is used for the calculation of free boundaries.

5.2 Comparison of asymptotic and numerical approximations

In order to numerically investigate the accuracy of the asymptotic approximation and compare to the finite difference PDE solutions in American type financial derivatives, we show the American put option values including XVA with mean-reversion counterparty default intensity, with the parameters of Table 1, except that we vary the speed of mean-reversion parameter, κ. We present Table 6, in which κ is varying from 1 to 5. This table can also help us numerically analyze how the asymptotic solution accuracy is affected by the speed of mean-reversion parameter κ. In Table 6, we keep $\nu = \sigma^{\lambda_C}\sqrt{\epsilon}$ constant, where $\kappa = \frac{1}{\sqrt{\epsilon}}$, and σ^{λ_C} is varying with varying κ. The exact solutions to these problems are not known. Therefore, we compute the numerical approximations by the 2D PDE approach and asymptotic approximations. Also, we compute a highly accurate numerical approximation extrapolated from the two finest grids of the 2D PDE approximations using Richardson extrapolation. The results by Richardson extrapolation are considered as the most accurate approximations. In Table 6, we notice, for points in the exercise region, both the 2D PDE solution (with high resolution) and the asymptotic give exact results within tolerance $\mathcal{O}(\frac{1}{p})$. In this case, Richardson extrapolation deviates from the exact results, as extrapolation brings wrong digits in the numerical 2D PDE solution beyond the seventh digit to the left. For these points, extrapolation with respect to the grid size does not make sense. For most points in the hold region, we notice that the agreement between the PDE and asymptotic solutions is in the third of higher significant decimal digit, and as κ increases there is stronger agreement.

	(7.5, 0.05)	(7.5, 0.1)	(15, 0.05)	(15, 0.1)	(30, 0.05)	(30, 0.1)
$\kappa = 1, \sigma^{\lambda_C} = 0.2, \nu = 0.2$						
PDE FDM	7.5000000	7.5000000	2.1750101	2.1403166	0.1216946	0.1194522
PDE extrap	7.5000001	7.5000000	2.1750516	2.1403572	0.1217110	0.1194685
asymptotic	7.5000000	7.5000000	2.1947775	2.1187456	0.1236463	0.1194102
$\kappa = 2, \sigma^{\lambda_C} = 0.28, \nu = 0.2$						
PDE FDM	7.5000000	7.5000000	2.1756124	2.1497291	0.1217586	0.1202117
PDE extrap	7.5000001	7.5000000	2.1756538	2.1497695	0.1217750	0.1202280
asymptotic	7.5000000	7.5000000	2.1879855	2.1499696	0.1228682	0.1207502
$\kappa = 3, \sigma^{\lambda_C} = 0.35, \nu = 0.2$						
PDE FDM	7.5000000	7.5000000	2.1758164	2.1556302	0.1217499	0.1205987
PDE extrap	7.5000001	7.5000000	2.1758578	2.1556707	0.1217664	0.1206150
asymptotic	7.5000000	7.5000000	2.1850350	2.1596910	0.1225268	0.1211148
$\kappa = 4, \sigma^{\lambda_C} = 0.4, \nu = 0.2$						
PDE FDM	7.5000000	7.5000000	2.1758642	2.1595322	0.1217224	0.1208164
PDE extrap	7.5000001	7.5000000	2.1759056	2.1595729	0.1217389	0.1208328
asymptotic	7.5000000	7.5000000	2.1832931	2.1642851	0.1223242	0.1212652
$\kappa = 5, \sigma^{\lambda_C} = 0.45, \nu = 0.2$						
PDE FDM	7.5000000	7.5000000	2.1758420	2.1622297	0.1216910	0.1209478
PDE extrap	7.5000001	7.5000000	2.1758835	2.1622708	0.1217075	0.1209643
asymptotic	7.5000000	7.5000000	2.1821117	2.1669053	0.1221864	0.1213391

Table 6: Values of $\hat{V}$ at several points (S, λ_C) and by different approaches for American put option including bilateral XVA with stochastic default intensity on counterparty with the parameters in Table 1, except that κ varies as indicated, and $\sigma^{\lambda_C} = 0.2\sqrt{\kappa}$. The grid size for the PDE solution is $N = 512, M = 256$, and extrapolation takes place between $N = 256, M = 128$ and $N = 512, M = 256$.

In Figure 2, top, we plot the "errors" of the PDE and the asymptotic solutions versus κ. The PDE solution is calculated with $N = 512, M = 256$. The errors are approximated by the difference between the respective approximations and the PDE extrapolated solution. From Figure 2, we can see the errors of the asymptotic solutions are decreasing with increasing κ at some constant order with few fluctuations, while the errors of the PDE solution are κ-independent. The latter errors are mainly affected by the S-points of evaluation, and are larger on the strike K than far away. Numerically, we observe that the order of convergence of asymptotic solution with respect to κ^{-1} is approximately 0.75. We believe that the reason why this order is lower than in the European case, is that the free boundary approximation is of low order.

In Figure 2, bottom, we present a similar plot, but versus the grid size N. As expected, the PDE solution converges (at order 2) with N, exhibiting the same accuracy for different κ, while the asymptotic solution accuracy is unaffected by N. However, the asymptotic solution is again more accurate for S away from the strike and for larger κ. The asymptotic solution is more accurate than the PDE one for small values of N (e.g. $N = 64$), S away from the strike, and larger values of κ. Clearly, the asymptotic solution is a lot more efficient than the PDE one in all cases, as it involves the PDE solution of an 1D problem and a few explicit formulae.

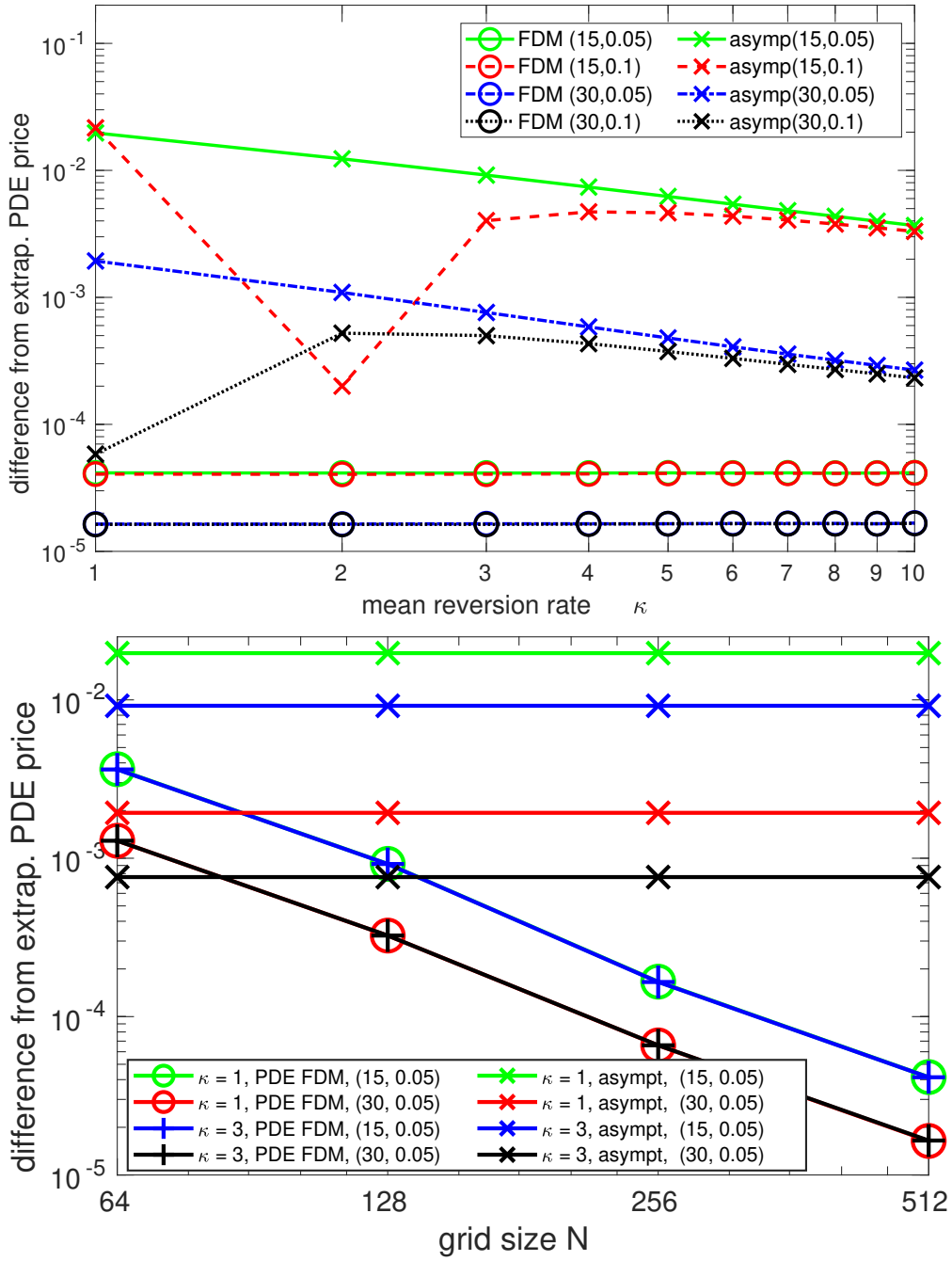

Figure 2: Accuracy comparison between 2D PDE and asymptotic approximations for American put option valuation including bilateral XVA assuming stochastic default intensity on counterparty with the parameters in Table 1, except κ as indicated, and $\sigma^{\lambda_C} = 0.2\sqrt{\kappa}$. Top is accuracy versus κ, with $N = 512, M = 256$ for the PDE solution. Bottom is accuracy versus N, with κ as indicated in the legend.

In Table 7, we also compare the free boundary locations computed by the numerical 2D PDE solutions at specific λ_C points, and with various κ values, with those computed by the asymptotic approach (which vary with κ, but not with λ_C). As mentioned in the previous subsection, the free boundary location changes very little with respect to κ when $\lambda_C = 0.05$. Considering the 2D PDE approach, when λ_C is

less than the mean, the free boundaries are increasing with κ, while when λ_C is larger than the mean, the free boundaries are decreasing with κ. Furthermore, in the case that λ_C is away from the mean, the differences of free boundaries between the numerical PDE and asymptotic approximations become smaller as κ increases, because of the mean-reversion effects.

κ	1	2	3	4	5
$\lambda_C = 0.025$					
PDE FDM	8.1536824	8.1766449	8.1935013	8.2090283	8.2205320
asymptotic	8.3312995	8.3317912	8.3320091	8.3321389	8.3322275
difference	-1.78e-01	-1.55e-01	-1.39e-01	-1.23e-01	-1.12e-01
$\lambda_C = 0.05$					
PDE FDM	8.3647338	8.3682853	8.3687280	8.3681869	8.3672369
asymptotic	8.3312995	8.3317912	8.3320091	8.3321389	8.3322275
difference	3.34e-02	3.65e-02	3.67e-02	3.60e-02	3.50e-02
$\lambda_C = 0.1$					
PDE FDM	8.7032745	8.6694023	8.6429295	8.6238303	8.6075403
asymptotic	8.3312995	8.3317912	8.3320091	8.3321389	8.3322275
difference	3.72e-01	3.38e-01	3.11e-01	2.92e-01	2.75e-01

Table 7: Comparison of free boundary locations given by different approaches at various λ_C points for American put option including bilateral XVA with the parameters in Table 1, except that κ varies as indicated, and $\sigma^{\lambda_C} = 0.2\sqrt{\kappa}$. The grid size for the PDE solution is $N = 512, M = 256$. Algorithms 1 and 2 are used for the calculation of free boundaries for the (2D) PDE FDM and the asymptotic methods, respectively.

5.3 Comparison of American and European type XVA

In order to compare the American and European put options with XVA, we solve the respective problem for European case, considering the same parameter settings, as shown in Table 1, and produce results for European options to be compared to the results in Tables 2 and 3 for American options. The results for European options are presented in Tables 8 and 9. Comparing the results of Tables 2 and 6, we easily see that the average number of iterations in each timestep is about 1.1 to 1.2 for European options, which is smaller than the ones for American options. We expect smaller number of iterations for European derivatives, since the American case has more nonlinearity. Also, for American derivatives, the average of number of iterations depends a little more on problem size than for the European case. Furthermore, from Tables 2, 3, 8 and 9, we can directly observe that the American derivative including XVA has slightly larger values than the European one, which is expected from the nature of American derivatives.

N	M	N_t	iter tot	iter avg	$\hat{V}$ value for put option		
					value	diff in $\hat{V}$	order
16	8	10	12	1.20	2.0790884	–	–
32	16	18	22	1.22	2.1114901	3.24e-02	–
64	32	34	40	1.18	2.1196343	8.14e-03	1.99
128	64	66	77	1.17	2.1218013	2.17e-03	1.91
256	128	130	150	1.15	2.1223410	5.40e-04	2.01
512	256	258	297	1.15	2.1224747	1.34e-04	2.01
Richardson extrapolated value: 2.1225193							

Table 8: Results for European put option including bilateral XVA with stochastic default intensity on counterparty using the penalty-like algorithm in [8] with the parameters in Table 1 when S is at-the-money ($S = K = 15$) and $\lambda_C = \theta$. Nonuniform grids are used.

N, M, N_t	(7.5, 0.025)	(7.5, 0.05)	(7.5, 0.1)	(30, 0.025)	(30, 0.05)	(30, 0.1)
128, 66, 68	6.9954401	6.9205456	6.7723182	0.1215826	0.1204373	0.1180971
256,128,130	6.9956602	6.9207611	6.7725231	0.1218132	0.1206653	0.1183202
512,256,258	6.9957152	6.9208149	6.7725743	0.1218705	0.1207220	0.1183757
order	2.00	2.00	2.00	2.01	2.01	2.01

Table 9: Results at various points (S, λ_C) for European put option including bilateral XVA with stochastic default intensity on counterparty using the penalty-like algorithm in [8] with the parameters in Table 1 at various points. Nonuniform grids are used.

6 Conclusions

We formulated and studied, from a perspective of computation issues, the bilateral XVA pricing of American-type financial derivatives, with focus on American put options, assuming stochastic counterparty default intensity. We formulated a 2D time-dependent linear complementarity PDE problem, reformulated it into a 2D time-dependent PDE with multiple nonlinear source terms, and developed two approaches to numerically approximate the option's value and free boundary. For the first approach, the direct numerical 2D PDE approximation, we used Algorithm 3 in [8] with the matrices adjusted as described in Section 3.2 for handling the nonlinear terms (one from XVA and another one from the American constraints). We also provided Algorithm 1 for the accurate calculation of the free boundary for any λ_C. For the second approach, the asymptotic approximation, we extended the asymptotic approximation formulation of XVA in European derivatives [9] to American derivatives, as well as developed the asymptotic approximation of the free boundary location. The asymptotic approximations to the price and the free boundary need the solution to the 1D American XVA PDE with constant counterparty default intensity, and a few corrections terms. We presented Algorithms 2 and 3 for the calculation of the correction terms, and the asymptotic approximations to the free boundary and the price. The numerical experiments show that the numerical 2D PDE approximation converges at stable second order in terms of the grid size, while the free boundary calculated based on it converges at order close to two. The asymptotic approximation price has a 0.75 convergence rate in terms of κ^{-1}, however, it is at least one order more efficient than the numerical 2D PDE approximation, so that, in some cases, it is preferable to use.

Regarding future research directions, for the American XVA problem, it is interesting to study the error of the asymptotic formula of the free boundary approximation, as the range of the untrusted area around the approximated free boundary is important in the XVA pricing problem. It is also interesting to

improve the accuracy of the asymptotic approximation of free boundary to the same accuracy level of the asymptotic approximation of price, which is at least $\mathcal{O}(\epsilon^{3/2})$. This may need one or two more correction terms to our existing asymptotic approximation.

In addition, XVA pricing often involves multiple assets in a portfolio. This results in a problem with many dimensions. It would be interesting to study some modern approximation techniques, such as machine learning and neural network approaches, for this XVA problem. We hope that such techniques will provide reasonable accuracy solutions, while overcome the curse of dimensionality.

7 Acknowledgments

The first author's work was supported in part by an OGS (Ontario Graduate Scholarship). The second aurhor's work was supported in part by the NSERC Discovery Grant RGPIN-2021-03502.

References

[1] A. AGARWAL, S. JUNEJA, AND R. SIRCAR, *American options under stochastic volatility: control variates, maturity randomization & multiscale asymptotics*, Quantitative Finance, 16 (2016), pp. 17–30.

[2] I. ARREGUI, B. SALVADOR, D. ŠEVČOVIČ, AND C. VÁZQUEZ, *Total value adjustment for European options with two stochastic factors: Mathematical model, analysis and numerical simulation*, Computers and Mathematics with Applications, 76 (2018), pp. 725–740.

[3] ——, *PDE models for American options with counterparty risk and two stochastic factors: Mathematical analysis and numerical solution*, Computers and Mathematics with Applications, 79 (2020), pp. 1525 – 1542.

[4] C. BURGARD AND M. KJAER, *In the balance*, Risk, 24 (2011), pp. 72–75.

[5] C. BURGARD AND M. KJAER, *Partial differential equation representations of derivatives with bilateral counterparty risk and funding costs*, The Journal of Credit Risk, 7 (2011), pp. 75–93.

[6] C. BURGARD AND M. KJAER, *The FVA debate: In theory and practice*, https://papers.ssrn.com/sol3/papers.cfm?abstract_id=2157634, (2012).

[7] ——, *Funding strategies, funding costs*, Risk, 26 (2013), pp. 82–87.

[8] Y. CHEN AND C. C. CHRISTARA, *Penalty methods for bilateral XVA pricing in European and American contingent claims by a PDE model*, Journal of Computational Finance, 24 (2021), pp. 41–70.

[9] ——, *Bilateral XVA pricing under stochastic default intensity: PDE modelling and computation*, Applied Numerical Mathematics, 185 (2023), pp. 236–259.

[10] P. A. FORSYTH AND K. R. VETZAL, *Quadratic convergence for valuing American options using a penalty method*, SIAM J. Sci. Comput., 23 (2002), pp. 2095–2122.

[11] J.-P. FOUQUE, G. PAPANICOLAOU, AND K. R. SIRCAR, *Derivatives in financial markets with stochastic volatility*, Cambridge University Press, 2000.

[12] ——, *From the implied volatility skew to a robust correction to Black-Scholes American option prices*, International Journal of Theoretical and Applied Finance, 4 (2001), pp. 651–675.

[13] J. P. FOUQUE, G. PAPANICOLAOU, R. SIRCAR, AND K. SOLNA, *Singular perturbations in option pricing*, SIAM J. Appl. Math., 63 (2003), pp. 1648–1665.

[14] N. C.-H. LEUNG, C. CHRISTARA, AND D. M. DANG, *Partial differential equation pricing of contingent claims under stochastic correlation*, SIAM J. Sci. Comput., 40 (2018), pp. B1–B31.

[15] D. WANG, K. SERKH, AND C. CHRISTARA, *A high-order deferred correction method for the solution of free boundary problems using penalty iteration, with an application to American option pricing*, Journal of Computational and Applied Mathematics, 432-115272 (2023), pp. 1–26.

[16] M. WIDDICKS, P. W. DUCK, A. D. ANDRICOPOULOS, AND D. P. NEWTON, *The Black-Scholes equation revisited: Asymptotic expansions and singular perturbations*, Mathematical Finance: An International Journal of Mathematics, Statistics and Financial Economics, 15 (2005), pp. 373–391.